




# Analysis of the geometry of the zero-velocity curves in the $N$ -body ring problem depending on the mass ratio parameter

Zahra Boureghda<sup>a</sup> , M. C. Martínez-Belda<sup>b</sup> , Juan F. Navarro<sup>c</sup> 

Department of Applied Mathematics, University of Alicante, Alicante, Spain

Received: 4 October 2023 / Accepted: 1 January 2024  
© The Author(s) 2024

**Abstract** The purpose of the present study is the investigation of the effect of the mass ratio parameter,  $\beta$ , on the geometry of the zero-velocity curves, when there are  $N = 3, 4, \dots, 100$  peripheral bodies. It is well known that there is a bifurcation value of the  $\beta$  parameter in the  $N$ -body ring problem that produces a change in the number of stationary solutions in the system from  $5N$  to  $3N$ . By examining the behavior of the critical values of the Jacobi constant that define each of the zones of stationary solutions, we have unveiled the existence of other bifurcations or critical values of  $\beta$  in the scenario with  $5N$  stationary solutions, which cause different changes in the geometry of the zero-velocity curves, which in turn affect the threshold for the total opening of the curves of zero velocity.

## 1 Introduction

For decades, the  $N$ -body problem has captivated the interest of scientists, to investigate and improve the comprehension of various celestial phenomena, such as exoplanetary systems, the Saturn's rings, and Trojan asteroids. These scientific investigations provide a contemporary challenge in unraveling the processes of Solar System formation. Besides that, recent researches have seen an increase in the amount of effort devoted to understanding the dynamics of these celestial bodies, near their equilibrium points, since these points can maintain a relatively stable position. This fact has led to design and develop several space exploration missions with numerous benefits [1], such as the launch of the James Webb Space Telescope (JWST) in 2021, that uses a special type of orbits, known as *halo orbits* of the Sun-Earth system [2, 3], and the satellites Genesis, SOHO, MAP, and ACE [4].

The first approximation of the  $N$ -body problem was presented by Maxwell in his investigation of Saturn's rings [5] on the so-called restricted  $N$ -body problem, which deals with the motion of a small particle under the gravitational influence of  $N + 1$  bodies in a planar ring configuration. Several authors have carried out qualitative research to improve our understanding on the behavior of the motion of that small body in a complex physical system [6–19]. For instance, [8] and [11] studied the equilibrium points and the zero-velocity curves (i.e., the contour lines that limit the zones where the particle's motion is allowed, denoted as ZVC in the following), distinguishing between the presence or not of a central body and unveiling a bifurcation in the number of stationary solutions based on the mass ratio parameter  $\beta$ ; [10] determined the stability of the stationary solutions and their parametric variations, extending the problem to the case when the central primary is assumed to be ellipsoidal or a source of radiation, founding also bifurcations depending on  $\beta$ ; [13] made a review of the change of the equilibrium points, their stability, and bifurcation points, and used new techniques to delimit the regions of chaotic behavior, classifying different kinds of orbits (escape, collision, and bounded orbits) and also obtaining new families of periodic orbits for some values of  $N$ ; [15–18] studied the escape dynamics through the use of surfaces of a section unveiling structures in the basins of escape dealing with the stable and unstable manifolds of the unstable Lyapunov orbits present in the windows of escape of the potential well; [20, 21] investigated the effects of introducing perturbation parameters such as radiation source; [19] considered the impact of small perturbations in the Coriolis and centrifugal forces, for  $N = 4, 7, 32$ , in order to numerically illustrate the effect of different parameters on the existence of equilibrium points and regions of motion; and [12] analyzed the shape of the ZVC depending on  $\beta$  for  $N = 10$  peripheral bodies, obtaining new critical values of  $\beta$  that affect the geometry of the ZVC. However, the influence of the parameters of the system in the geometry of the ZVC when  $N$  increases is far from being completely unveiled. The existing studies present certain limitations in the prediction of the behavior of the ZVC depending on the mass ratio parameter and the Jacobi constant of the system, as the number of peripheral bodies affects the system dynamics.

<sup>a</sup> e-mail: [zb21@alu.ua.es](mailto:zb21@alu.ua.es)

<sup>b</sup> e-mail: [carmen.martinez@ua.es](mailto:carmen.martinez@ua.es) (corresponding author)

<sup>c</sup> e-mail: [jf.navarro@ua.es](mailto:jf.navarro@ua.es)

The purpose of the present study is to do an extensive and qualitative study of the ZVC in the planar  $N$ -body ring problem for an increasing number of the peripheral bodies, up to  $N = 100$ , depending on the values of  $\beta$  and the Jacobi constant under the presence of a central primary, that is, when  $\beta > 0$ , and considering spherical and homogeneous primaries with equal masses. In Sect. 2, we provide a brief summary of the equations of motion of a particle subject to the gravity field of a  $N$ -body ring arrangement revolving around a central mass. Section 3 presents a review of the location and linear stability of the stationary solutions of this dynamical system. In Sect. 4, we focus on the study of the ZVC, discussing the influence of the mass ratio parameter,  $\beta$ , on their geometry for the values of  $N$  mentioned above. Finally, in the last section, we extract the conclusions and give future perspectives of this investigation.

## 2 The general equations of motion

Let us assume a reference frame spinning at an angular velocity equal to the unit, with its origin corresponding toward the main body's center of mass and the  $x$  axis fixed along the line connecting the center mass to a single of the primaries in the ring. The non-dimensional equations of motion characterizing the planar motion of a particle  $S$  of infinitesimal mass (hence referred to as the test particle) under the effect of this configuration are defined by [see, for instance, 8, 9]:

$$\ddot{x} - 2\dot{y} = \frac{\partial U}{\partial x}, \quad \ddot{y} + 2\dot{x} = \frac{\partial U}{\partial y}. \quad (1)$$

The potential function  $U(x, y)$  is described by the following general expression

$$U(x, y) = \frac{1}{2}(x^2 + y^2) + \frac{1}{\Delta} \left( \frac{\beta}{r_0} + \sum_{v=1}^N \frac{1}{r_v} \right),$$

where  $\beta = m_0/m$  represents the ratio of the central mass,  $m_0$ , with one of the peripheral masses,  $m$ ,

$$r_0 = \sqrt{x^2 + y^2}$$

is the test particle's distance from the central body,

$$r_v = \sqrt{(x - x_v^*)^2 + (y - y_v^*)^2},$$

for  $v = 1, 2, \dots, N$ , are the distances between the test particle and the  $N$  peripheral primaries of the system, while the quantities  $x_v^*$  and  $y_v^*$  represent the positions of the peripheral bodies, which are written as

$$x_v^* = \frac{1}{2 \sin \theta} \cos(2(v-1)\theta), \quad y_v^* = \frac{1}{2 \sin \theta} \sin(2(v-1)\theta).$$

Lastly, the parameter  $\Delta$  is defined by

$$\Delta = M(\Lambda + \beta M^2),$$

where

$$\Lambda = \sum_{v=2}^N \frac{\sin^2 \theta \cos((N/2 + 1 - v)\theta)}{\sin^2((N + 1 - v)\theta)} = \sum_{v=2}^N \frac{\sin^2 \theta}{\sin((v-1)\theta)},$$

and

$$M = \sqrt{2(1 - \cos \psi)} = 2 \sin \theta.$$

In such expressions,  $\psi$  represents the angle between both the central and two succeeding peripheral primaries, and  $\theta = \psi/2 = \pi/N$ . It is straightforward to demonstrate that the set of equations (1) has a Jacobi-type integral of motion, determined by

$$C = 2U(x, y) - (\dot{x}^2 + \dot{y}^2), \quad (2)$$

in which  $C$  is the constant of Jacobi.

The regions of the test particle's possible motion are bounded by the zero-velocity curves, which are obtained from equation (2), and read as follows:

$$C = 2U(x, y) = x^2 + y^2 + \frac{2}{\Delta} \left( \frac{\beta}{r_0} + \sum_{v=1}^N \frac{1}{r_v} \right). \quad (3)$$

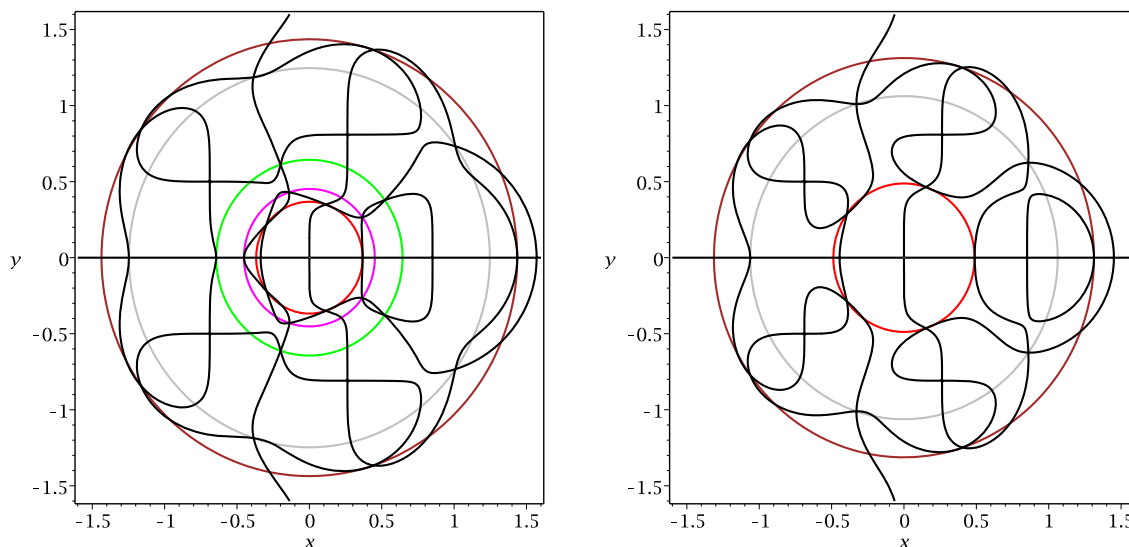


**Fig. 1** Partial derivatives of  $U(x, y)$  for  $N = 5$ ,  $\beta = 0.5$  (left panel), and  $N = 5$ ,  $\beta = 2.0$  (right panel), depicted in black color. The critical points are organized in equal arcs on concentric circumferences from the center. For  $\beta = 0.5$  there are five circumferences and for  $\beta = 2.0$  there are three of them, depicted in red, magenta, green, gray and brown colors

### 3 Zones of stationary solutions

The stationary solutions of this dynamical system, that is, its equilibrium points, satisfy the following nonlinear system

$$\frac{\partial U}{\partial x} = 0, \quad \frac{\partial U}{\partial y} = 0. \tag{4}$$

Therefore, they are the critical points of the potential function  $U(x, y)$ , as well. Note also that the potential function has multiple symmetries: it is symmetric with respect to the line from the center to every peripheral body as well as to the line from the origin to the bisector across adjacent primaries. Then, in order to determine the location of the critical points of  $U(x, y)$ , it is enough to focus on the angular portion  $[0, \pi/N]$ . Equation (4) can be solved numerically, for instance, by means of the Newton–Raphson method, and the critical points can be classified by studying the sign of the Hessian matrix of  $U(x, y)$ .

Due to the fact that the stationary points satisfy the equation of the integral of motion of the system (3), they are also characterized by a particular value of the constant of Jacobi,  $C$ , which will be here named as *critical value of C*. Then, we can classify the stationary points attending to their associated critical value of  $C$ . According to [8], when  $\beta > 0$ :

- The stationary solutions are organized at the intersections of concentric circumferences with radial lines generating equal angles  $\pi/N$  between them due to the symmetries of the potential function.
- The stationary points can be grouped in subsets of  $N$  points such that all the points in the subset belong to the same circumference, that is, each  $N$  equilibrium points are at the same distance from the center. Then, each subset of points with the same radius defines a *zone* and it is associated with the same critical value of the Jacobi constant.
- The number of stationary solutions depends on  $N$  and  $\beta$ , and the radii of the different zones increase as  $N$  increases.
- There can be from a minimum of three to a maximum of five zones, each of them containing  $N$  equilibrium points. We shall refer to them as zones  $A_1, A_2, B, D_1$ , and  $D_2$ , with associated critical value of the constant of Jacobi denoted as  $C_{A_1}, C_{A_2}, C_B, C_{D_1}$ , and  $C_{D_2}$ , respectively. These critical values can be computed by means of equation (3).
- There are always  $N$  points in each zone, but the number of zones varies depending on the value of the mass ratio parameter,  $\beta$ . There exists a value  $\beta_N^*$  for each  $N$  such that, there are five zones when  $\beta$  is in the interval  $(0, \beta_N^*)$ , and there are three zones when  $\beta > \beta_N^*$ , which are  $A_1, D_1$ , and  $D_2$ . When  $\beta = \beta_N^*$  there are  $4N$  equilibrium points. That is, there is a bifurcation in the  $N$ -body problem depending on the mass ratio parameter,  $\beta_N^*$ , such that there is a variation from  $5N$  to  $3N$  total number of stationary solutions in the system.

In Fig. 1, we show two examples of the curves that result for the partial derivatives of  $U(x, y)$  (equations (4)), as well as the circumferences containing the equilibrium points, when  $N = 5$  and  $\beta = 0.5, 2.0$ . In the first case, there are  $5N$  equilibrium points, that is, five zones, whereas in the second one, there are  $3N$  equilibrium points, that is, there are three zones.

The bifurcation value of  $\beta$  for each  $N$ ,  $\beta_N^*$ , can be found numerically following the procedure described in [19]. In Table 1, we show the total number of stationary solutions and the range of values allowed for  $\beta$  in each case for several values of  $N$ . It can be remarked that the length of the interval  $(0, \beta_N^*)$  such that the corresponding dynamical system has  $5N$  equilibrium points increases when  $N$  increases.

**Table 1** Intervals of  $\beta$  such that the system has  $5N$  or  $3N$  stationary solutions for several values of  $N$ 

$N$	$5N$ stat. sol. ( $0, \beta_N^*$ )	$3N$ stat. sol. ( $\beta_N^*, +\infty$ )
3	(0,0.014021)	(0.014021, $\infty$ )
4	(0,0.18708)	(0.18708, $\infty$ )
5	(0,0.67771)	(0.67771, $\infty$ )
6	(0,1.6084)	(1.6084, $\infty$ )
7	(0,3.0988)	(3.0988, $\infty$ )
8	(0,5.2731)	(5.2731, $\infty$ )
9	(0,8.2558)	(8.2558, $\infty$ )
10	(0,12.16)	(12.16, $\infty$ )
11	(0,17.13)	(17.13, $\infty$ )
12	(0,23.26)	(23.26, $\infty$ )
13	(0,30.7561)	(30.7561, $\infty$ )
14	(0,39.58)	(39.58, $\infty$ )
15	(0,50.02)	(50.02, $\infty$ )
16	(0,62.11)	(62.11, $\infty$ )
17	(0,76.05)	(76.05, $\infty$ )
18	(0,91.91)	(91.91, $\infty$ )
19	(0,109.83)	(109.83, $\infty$ )
20	(0,129.92)	(129.92, $\infty$ )
32	(0,592.8242)	(592.8242, $\infty$ )

The pattern of the location of the equilibrium points for each zone is also known. Due to the symmetries of the potential function, all the equilibrium points are placed either in the line that joins the origin with any of the primaries or in the line from the center to the bisector of two consecutive primaries. The characteristics of each of the possible zones are as follows [see, for instance, 8]:

- The closest zone to the origin (denoted as  $A_1$ ) represents the stationary points which lie on the lines connecting the central body with a peripheral primary and they are located between them. These points are known as *inner collinear* points.
- The second closest zone to the origin (denoted as  $A_2$ ) represents the stationary points which relate the bisector between two successive primaries and are between the central body and the primaries. These points are known as *inner between-masses* points.
- The third zone (denoted as  $B$ ) comprises the stationary points which lie also on the same bisector but are between two successive peripheral primaries. These points are known as *peripheral between-masses points*.
- The fourth zone (denoted as  $D_2$ ) contains the stationary points which lie also on the bisector between two subsequent peripheral primaries, but independent of them. These points are known as *outer island* points.
- The outermost zone (denoted as  $D_1$ ) represents the stationary points that relate with the identical lines as the primary zone; however, they are not part of the peripheral primaries. These points are known as *outer collinear* points.

When  $\beta$  grows, the zone delimited by the *inner between-masses*,  $A_2$ , and the one created by the *peripheral between-masses*,  $B$ , approach each other up to the bifurcation point  $\beta_N^*$ , where they both disappear. Besides, when  $\beta \rightarrow \infty$ , the radii of the three zones that remain tend to the radius of the ring,  $r_N = 1/(2 \sin \theta) = 1/M$  [13]. Note that the radius of the ring gets bigger with  $N$ .

In Fig. 2, we illustrate the evolution of the zero-velocity curves and the location of the stationary solutions for  $N = 5$  and the mass ratio values  $\beta = 0.5$  and  $2.0$ , which belong to the intervals  $(0, \beta_N^*)$  and  $(\beta_N^*, +\infty)$ , respectively. The red asterisks mark the position of the *inner collinear* stationary points (zone  $A_1$ ), the *inner between-masses* points are depicted with magenta crosses (zone  $A_2$ ), the green boxes mark the location of the *peripheral between-masses* points (zone  $B$ ), the *outer island* points are plotted with gray diamonds (zone  $D_2$ ), and the brown circles mark the position of the *outer collinear* points (zone  $D_1$ ).

### 3.1 The stability condition of the equilibrium points

The stability of the equilibrium points determined by Eq. (4), can be analyzed by finding the roots of the following characteristic equation:

$$\lambda^4 + (4 - U_{xx} - U_{yy})\lambda^2 + (U_{xx}U_{yy} - U_{xy}^2) = 0. \quad (5)$$

An equilibrium point is said to be linearly stable if the eigenvalues of the characteristic equation are purely imaginary [22]. Several authors [13, 23–25] have studied their linear stability, which permits us to recall the next proposition:

**Theorem 1** *The equilibrium points of the  $(N + 1)$ -body ring problem satisfy the following properties:*

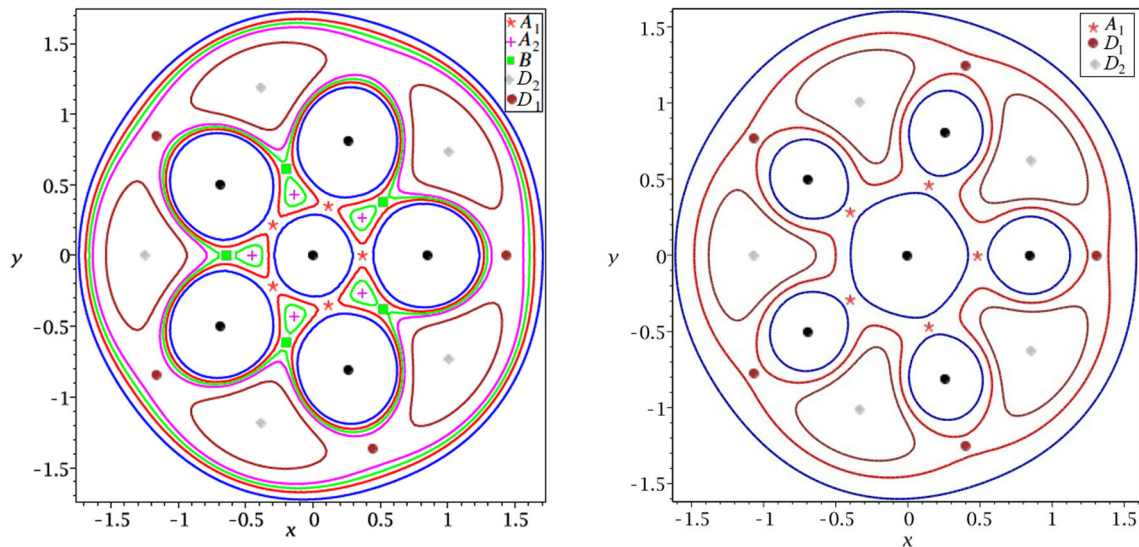


**Fig. 2** Zero-velocity curves and stationary points for  $N = 5$  and  $\beta = 0.5, 2.0$ . On the left panel, for  $\beta = 0.5$ , we show an example of each of the five different stages of the zero-velocity curves, as well as the location of the 25 stationary points. On the right panel, for  $\beta = 2.0$ , we show an example of each of the three different stages of the zero-velocity curves and the location of the 15 stationary points. The stationary points that belong to the same circumference (zone) are plotted with the same symbol and color. The primaries are depicted with black dots

- i) The equilibrium points that are located in zones  $A_1, B,$  and  $D_1$  are always unstable.
- ii) For all  $N$ , there exists a  $\beta_1(N)$  such that if  $\beta > \beta_1(N)$  the equilibrium points located in zone  $D_2$  are stable, with

$$\beta_1(N) = \frac{7(13 + 4\sqrt{10}) I(3) N^3}{4\pi^3},$$

where

$$I(3) = \sum_{k=1}^{+\infty} \frac{1}{k^3}.$$

- iii) The equilibrium points of zone  $A_2$  are stable if and only if the following conditions are satisfied:

$$\begin{aligned} & - N > 10930, \\ & - \beta < \frac{2N+S}{4} \left( \frac{27}{4(S/N-6)} \right)^{-3/2}, \end{aligned}$$

where  $S = \frac{2N}{\pi} \log \left( \frac{2N}{\pi} e^\gamma \right) - \frac{\pi}{36N} + O(1/N^2)$ , and  $\gamma$  stands for the Euler constant.

#### 4 The zero-velocity curves and their relation with $\beta$

In order to fulfill the main objective of this research, we have carried out an extensive analysis of the geometry of the zero-velocity curves for several values of  $\beta$  in the intervals  $(0, \beta_N^*)$  and  $(\beta_N^*, +\infty)$ , for  $N = 3, 4, \dots, 100$ . The zero-velocity curves are characterized by three parameters: the number of peripheral primaries,  $N$ , the mass ratio parameter,  $\beta$ , and the constant of Jacobi,  $C$ . From a first analysis of the zero-velocity contours for several values of  $\beta$ , we can extract the following conclusions:

- When  $\beta > \beta_N^*$ , there are only three (different) critical stages of the zero-velocity curves, which are in accordance with the three different zones ( $A_1, D_2,$  and  $D_1$ ) created by the stationary solutions (see the right panel of Fig. 2). In this scenario, the zero-velocity curves are topologically equivalent when the value of the Jacobi constant decreases for different values of  $\beta$ .
- When  $0 < \beta < \beta_N^*$ , there are five (different) critical stages of the zero-velocity contours, which are in accordance with the five different zones ( $A_1, A_2, B, D_2,$  and  $D_1$ ) created by the stationary solutions (see the left panel of Fig. 2). However, contrarily to the previous scenario, the transitions in the zero-velocity curves when value of the Jacobi constant decreases present a different pattern depending on  $\beta$ .

A deeper analysis of the influence of  $\beta$  on the evolution of the zero-velocity curves when  $0 < \beta < \beta_N^*$  unveils that there are some critical values of  $\beta$  in the  $N$ -body ring problem that are directly related to the different patterns of the zero-velocity curves in this scenario, as we will explain in the next section.

**Table 2** Values of  $\beta_{E_i}$ , for  $i = 1, 2, \dots, 7$ , for several values of  $N$  from 3 to 100

$N$	$\beta_{E_1}$ $C_{A_1} = C_{D_2}$	$\beta_{E_2}$ $C_{D_2} = C_{A_2}$	$\beta_{E_3}$ $C_{D_1} = C_{A_1}$	$\beta_{E_4}$ $C_{D_1} = C_{A_2}$	$\beta_{E_5}$ $C_B = C_{A_1}$	$\beta_{E_6}$ $C_{D_1} = C_{A_2}$	$\beta_{E_7}$ $C_B = C_{D_1}$
3	–	–	–	–	0.00642192204	–	–
4	–	–	–	0.0211687364	0.1056265308	–	–
5	0.0145514611	0.01464692201	0.1369728160	0.1545667160	0.4085592184	–	–
6	0.1459689364	0.14889593300	0.379749559	0.4316140001	0.9962877306	–	–
7	0.4142013834	0.42549434600	0.7748770500	0.884634632	1.941930973	2.981730512	3.004145950
8	0.8384906000	0.86529626070	1.349449902	1.548632560	3.316234786	4.433851700	4.712717720
9	1.4401360100	1.49136944800	2.130267000	2.461349210	5.188900200	6.174944211	6.981986165
10	2.2406440000	2.3272540000	3.143930200	3.664162200	7.629044000	8.21202000	9.484532727
11	3.26142052000	3.396645600	4.416923040	5.203657260	10.70540910	10.54097200	13.45723370
12	4.5236971800	4.723304610	5.975656480	7.134380950	14.48647910	13.14746300	17.79742110
13	6.0485114800	6.331021370	7.846500000	9.524164300	19.04054615	16.0024440	22.96287172
14	7.8567035900	7.856703800	10.05579500	12.46617400	24.43575935	19.0504600	29.02136220
15	9.9689203500	10.48485800	12.62986400	16.11408300	30.74015400	22.17466000	36.04066800
16	12.405621050	13.07860610	15.59502202	20.85833604	38.02168000	25.02070420	44.08853809
17	15.187079000	16.04866200	18.97757011	–	46.34820800	–	53.23270200
18	18.333398100	19.41884300	22.80380910	–	55.78755050	–	63.54086020
19	21.864507200	23.21296156	27.10003340	–	66.40748000	–	75.08066880
20	25.800171400	27.45482601	31.89252614	–	78.27570080	–	87.91978320
30	91.651430000	99.73504210	112.8933603	–	280.4930500	–	302.6404040
40	218.69901000	242.9541000	272.4168100	–	681.8690000	–	721.5828000
50	424.76842000	480.8720012	536.7109740	–	1349.873540	–	1412.206042
60	726.89230000	837.2272000	932.0210430	–	2351.931710	–	2441.928150
70	1141.4900000	1335.770000	1484.580000	–	3755.451000	–	3878.153900
80	1684.4765000	2000.200000	2220.611000	–	5627.823000	–	5788.274500
90	2371.3619100	2854.260610	3166.342000	–	8036.430470	–	8239.670000
100	3217.2930000	3921.662000	4348.0000	–	11048.65600	–	11299.72500

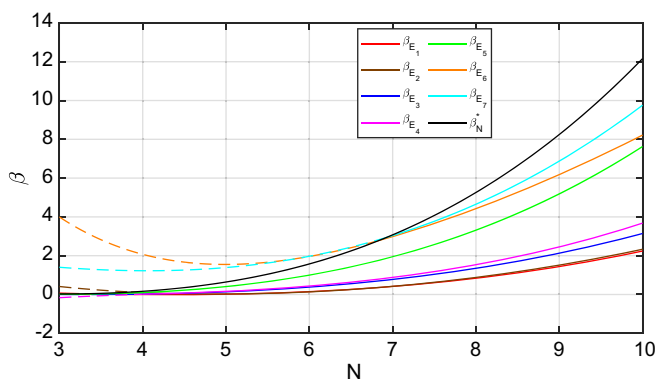
#### 4.1 Critical values of $\beta$ in the interval $(0, \beta_N^*)$

When  $\beta \in (0, \beta_N^*)$ , there exist some critical values that explain the differences in the transitional shapes of the zero-velocity curves. These critical values of the parameter  $\beta$  are found by studying the intersections of the curves that provide the relation between  $\beta$  and each of the five critical values of the Jacobi constant,  $C_{A_1}$ ,  $C_{A_2}$ ,  $C_B$ ,  $C_{D_2}$ , and  $C_{D_1}$ . The latter are obtained, as mentioned in Sect. 3, by computing numerically the stationary solutions of the system, that must satisfy the system of Eq. (4), and substituting them in Eq. (3), that is, each critical value  $C_j$  is associated with a set of stationary solutions of the system. In order to compute the critical values of  $\beta$  with a high level of precision, we used an algorithm based on the bisection method, implemented in the software Maple, so that we started by searching for an initial interval of  $\beta$  such that there is a change in the order of magnitude of two critical values of the Jacobi constant, that is, there is a change from  $C_i < C_j$  to  $C_i > C_j$  or vice versa, with  $i, j \in \{A_1, A_2, B, D_2, D_1\}$ ,  $i \neq j$ , and next we continuously narrowed down this interval up to a precision given by  $|C_i - C_j| \leq 10^{-10}$ , obtaining the critical value of  $\beta$  such that  $C_i = C_j$ .

Our analysis reveals that there can appear up to seven critical values of  $\beta$ , here named as  $\beta_{E_i}$ ,  $i = 1, 2, \dots, 7$ , which correspond, respectively, to the following intersections between the critical values of the Jacobi constant:  $C_{A_1} = C_{D_2}$ ,  $C_{A_2} = C_{D_2}$ ,  $C_{D_1} = C_{A_1}$ ,  $C_{A_2} = C_{D_1}$ ,  $C_B = C_{A_1}$ ,  $C_{A_2} = C_{D_1}$ , and  $C_B = C_{D_1}$ . Note that  $C_{A_2}$  and  $C_{D_1}$  can intersect twice, so that  $\beta_{E_4}$  and  $\beta_{E_6}$  stand for the first and the second intersections of  $C_{A_2}$  and  $C_{D_1}$ , respectively.

In Table 2, we show the values of  $\beta_{E_i}$  for several values of  $N$  in the interval [3, 100]. Let us observe that the maximum number of intersections occurs when  $7 \leq N \leq 16$ , and they satisfy the relation  $\beta_{E_i} < \beta_{E_{i+1}}$ , for  $i = 1, 2, \dots, 6$ , except when  $11 \leq N \leq 16$ , for which  $\beta_{E_5} > \beta_{E_6}$ , that is, the second intersection between  $C_{A_2}$  and  $C_{D_1}$  appears before the intersection between  $C_B$  and  $C_{A_1}$ . When there are three peripheral bodies, only the values of  $C_B$  and  $C_{A_1}$  intersect for some  $\beta$ , which corresponds to  $\beta_{E_5}$  in our notation; for  $N = 4$  only the values  $\beta_{E_4}$  and  $\beta_{E_5}$  appear; for  $N = 5, 6$  there appear just the first five intersections, that is,  $\beta_{E_i}$ , for  $i = 1, 2, \dots, 5$ , and they also verify that  $\beta_{E_i} < \beta_{E_{i+1}}$ ; and finally, for  $17 \leq N \leq 100$ , there are, as well, five intersections, but they correspond to the values  $\beta_{E_i}$ , for  $i = 1, 2, 3, 5, 7$ , which satisfy also the relation  $\beta_{E_1} < \beta_{E_2} < \beta_{E_3} < \beta_{E_5} < \beta_{E_7}$ .

**Fig. 3** Evolution of the bifurcation value of  $\beta$ ,  $\beta_N^*$ , and the critical values  $\beta_{E_i}$ ,  $i = 1, 2, \dots, 7$ , for  $3 \leq N \leq 10$ . The solid lines correspond to a polynomial interpolation of the existing values of  $\beta_{E_i}$ , for  $i = 1, 2, \dots, 7$ , and the dotted lines represent an extrapolation or prediction of these values when the intersection that they define does not happen



In Fig. 3, we show a plot of comparison between the evolution of the bifurcation value  $\beta_N^*$  and the critical values  $\beta_{E_i}$ , for  $i = 1, 2, 3, \dots, 7$ , when  $3 \leq N \leq 10$ , with colored solid lines. In addition, in dotted lines, we have depicted a prediction of the critical values of  $\beta$  for the values of  $N$  where they do not occur, by means of a polynomial interpolation. Let us observe that when the curves of  $\beta_{E_i}$  are below the curve of  $\beta_N^*$ , the critical values exist, whereas when they are above it (the dotted line corresponding to the extrapolated values), the critical values do not appear. This fact explains the absence of intersection between some zones for certain values of  $N$ . In summary, we can extract the following conclusions:

- The intersection values  $\beta_{E_i}$ ,  $i = 1, 2, 3$ , for  $N = 3, 4$ , and  $\beta_{E_4}$ , for  $N = 4$  do not appear due to the fact that the two inner zones  $A_1$  and  $A_2$  do not exist when  $\beta < \beta_0 \approx 0.001$  [12], and the critical values  $\beta_{E_i}$ , for  $i = 1, 2, 3, 4$ , which define the intersection of the zones  $A_1$  and  $A_2$  with the other zones, are expected to arise in such range of values.
- For  $N = 3, 4, 5, 6$ , the critical values  $\beta_{E_6}$  and  $\beta_{E_7}$  do not exist due to the fact that they are predicted to increase beyond the bifurcation value  $\beta_N^*$ , but in such case, the zones  $A_2$  and  $B$  disappear. Therefore, the intersections defined by  $\beta_{E_6}$  and  $\beta_{E_7}$  cannot occur because they involve the zone  $D_1$  with  $A_2$  and  $B$ , respectively.

In addition, we can conclude that for  $N > 16$ , the values  $\beta_{E_4}$  and  $\beta_{E_6}$  do not exist due to the fact that the adjacent zones  $A_1, A_2$  and  $D_1, D_2$  become too close to each other [8].

On the other hand, the critical values of  $\beta$  provide also information about the relation of order between the critical values of the Jacobi constant,  $C_i$ , for  $i = A_1, A_2, B, D_2, D_1$ , that define the different zones of stationary solutions. Indeed, for each sub-interval  $(\beta_{E_i}, \beta_{E_{i+1}})$  there is a fixed order in these values, which varies depending on the number of peripheral bodies,  $N$ . These different patterns are shown in Tables 3, 4, and 5. Note that they are in correspondence with the information provided by Table 2. We have also included in these tables the relation of order of the critical values of  $C$  when  $\beta > \beta_N^*$ , for which there are only the three zones  $A_1, D_2, D_1$ .

According to the information provided by these tables, we can set the following relations between the critical values of the Jacobi constant for  $N = 3, 4, 5, \dots, 100$ :

- For every  $\beta > 0$ , the relation  $C_{D_1} > C_{D_2}$  is always satisfied.
- For  $\beta \in (0, \beta_N^*)$ , the two extra zones that appear,  $A_2$  and  $B$  (which are not present if  $\beta > \beta_N^*$ ) always satisfy the relations  $C_{A_1} > C_{A_2}$ ,  $C_B > C_{A_2}$ , and  $C_B > C_{D_2}$ .
- For  $\beta > \beta_N^*$ , the relation  $C_{A_1} > C_{D_1} > C_{D_2}$  always holds, which explains the fact that the transitions in the shape of the zero-velocity curves for different values of  $C$  are topologically equivalent for different values of  $\beta$  and  $N$ .

Then, these relations are also consistent with the fact that there can only be up to a maximum of six different intersections between the values  $C_{A_1}, C_{A_2}, C_B, C_{D_2}$ , and  $C_{D_1}$  from a maximum of ten that could happen theoretically.

#### 4.2 Parametric evolution of the zero-velocity curves

As it has been mentioned previously, when  $0 < \beta < \beta_N^*$ , the critical transitions of the zero-velocity curves, defined by the five critical values of the Jacobi constant, are not topologically equivalent, that is, they evolve differently depending on the value of  $\beta$ . However, it is possible to identify a pattern with respect to this parameter depending on each of the sub-intervals that are created by the values  $\beta_{E_i}$ ,  $i = 1, 2, \dots, 7$ . In Figs. 4, 5, 6, 7, 8, and 9, we illustrate some examples of the zero-velocity curves for one value of  $\beta$  in each of the sub-intervals  $(\beta_{E_i}, \beta_{E_{i+1}})$ , for  $N = 8, N = 11$ , and  $N = 17$ , respectively. The graphs are ordered from the point of view of their associated value of the Jacobi constant, from highest to lowest values. The white regions denote the areas where the particle's motion is allowed whereas the motion is not possible in the gray ones. Our analysis reveal that the geometry of the zero-velocity curves is influenced by the appearance of each of the critical values  $\beta_{E_i}$ ,  $i = 1, \dots, 7$ , that is, they create certain effect in the shape of the zero-velocity curves. This effect is highlighted in Figs. 4, 5, 6, 7, 8 and 9 by coloring the boundary of the two consecutive panels or sub-figures where there is a change in the pattern of the zero-velocity curve, with a color code in accordance to Fig. 3, that is, the red, brown, blue, violet pink, green, orange, and cyan colors indicate the effect of  $\beta_{E_i}$ ,  $i = 1, \dots, 7$ , respectively.

**Table 3** Effect of the mass ratio parameter  $\beta$  on the arrangement of the critical values of the Jacobi constant  $C_{A_1}, C_{A_2}, C_B, C_{D_2}$ , and  $C_{D_1}$ , when  $N = 7, 8, 9, 10$

Sub-intervals created by the critical values of $\beta$	Order of the critical values of $C_i, i = A_1, A_2, B, D_2, D_1$
$\beta \in (0, \beta_{E_1})$	$C_B > C_{D_1} > C_{D_2} > C_{A_1} > C_{A_2}$
$\beta \in (\beta_{E_1}, \beta_{E_2})$	$C_B > C_{D_1} > C_{A_1} > C_{D_2} > C_{A_2}$
$\beta \in (\beta_{E_2}, \beta_{E_3})$	$C_B > C_{D_1} > C_{A_1} > C_{A_2} > C_{D_2}$
$\beta \in (\beta_{E_3}, \beta_{E_4})$	$C_B > C_{A_1} > C_{D_1} > C_{A_2} > C_{D_2}$
$\beta \in (\beta_{E_4}, \beta_{E_5})$	$C_B > C_{A_1} > C_{A_2} > C_{D_1} > C_{D_2}$
$\beta \in (\beta_{E_5}, \beta_{E_6})$	$C_{A_1} > C_B > C_{A_2} > C_{D_1} > C_{D_2}$
$\beta \in (\beta_{E_6}, \beta_{E_7})$	$C_{A_1} > C_B > C_{D_1} > C_{A_2} > C_{D_2}$
$\beta \in (\beta_{E_7}, \beta_N^*)$	$C_{A_1} > C_{D_1} > C_B > C_{A_2} > C_{D_2}$
$\beta > \beta_N^*$	$C_{A_1} > C_{D_1} > C_{D_2}$

In the following, we provide an extensive description of those effects, which have been organized by subsections depending on the number of peripheral primaries,  $N$ , for the shake of clarity.

4.2.1 Scenario with  $N < 11$

1.- When  $\beta \in (0, \beta_{E_1})$ :

- If  $C > C_B$ , the zero-velocity curves start determining an open outer space of motion and  $N + 1$  closed areas surrounding the primaries with no connection between them. Then, the particle is trapped, and the motion is only possible around the masses.
- If  $C_B > C > C_{D_1}$ , the particle may move from one peripheral primary to another because there are opened windows between the primaries. However, transport between the central body and the peripheral masses is not possible, owing to the fact that there appears an annulus around the central body.
- If  $C_{D_1} > C > C_{D_2}$ , the external closed area shrinks and decomposes into  $N$  isolated islands, creating  $N$  windows through which the particle can escape. However, there is still not possible escape from the center area as the annulus remains.
- If  $C_{D_2} > C > C_{A_1}$ , the  $N$  islands disappear, but the annulus remains.
- If  $C_{A_1} > C > C_{A_2}$ , the annulus that surrounded the center body opens into  $N$  small isolated islands, so that the particle can escape from the system.

2.- When  $\beta \in [\beta_{E_1}, \beta_{E_2})$ :

- The first three transitions, as well as the last one, are equivalent to the previous case.

**Table 4** Effect of the mass ratio parameter  $\beta$  on the arrangement of the critical values of the Jacobi constant  $C_{A_1}, C_{A_2}, C_B, C_{D_2}$ , and  $C_{D_1}$ , when  $N = 11, 12, \dots, 16$

Sub-intervals created by the critical values of $\beta$	Order of the critical values of $C_i, i = A_1, A_2, B, D_2, D_1$
$\beta \in (0, \beta_{E_1})$	$C_B > C_{D_1} > C_{D_2} > C_{A_1} > C_{A_2}$
$\beta \in (\beta_{E_1}, \beta_{E_2})$	$C_B > C_{D_1} > C_{A_1} > C_{D_2} > C_{A_2}$
$\beta \in (\beta_{E_2}, \beta_{E_3})$	$C_B > C_{D_1} > C_{A_1} > C_{A_2} > C_{D_2}$
$\beta \in (\beta_{E_3}, \beta_{E_4})$	$C_B > C_{A_1} > C_{D_1} > C_{A_2} > C_{D_2}$
<b><math>\beta \in (\beta_{E_4}, \beta_{E_6})</math></b>	<b><math>C_B &gt; C_{A_1} &gt; C_{A_2} &gt; C_{D_1} &gt; C_{D_2}</math></b>
<b><math>\beta \in (\beta_{E_6}, \beta_{E_5})</math></b>	<b><math>C_B &gt; C_{A_1} &gt; C_{D_1} &gt; C_{A_2} &gt; C_{D_2}</math></b>
<b><math>\beta \in (\beta_{E_5}, \beta_{E_7})</math></b>	<b><math>C_{A_1} &gt; C_B &gt; C_{D_1} &gt; C_{A_2} &gt; C_{D_2}</math></b>
$\beta \in (\beta_{E_7}, \beta_N^*)$	$C_{A_1} > C_{D_1} > C_B > C_{A_2} > C_{D_2}$
$\beta > \beta_N^*$	$C_{A_1} > C_{D_1} > C_{D_2}$

The bold stands for the changes in the order of the critical values of  $\beta$  with respect to the previous table

**Table 5** Effect of the mass ratio parameter  $\beta$  on the arrangement of the critical values of the Jacobi constant  $C_{A_1}, C_{A_2}, C_B, C_{D_2}$ , and  $C_{D_1}$ , when  $N = 16, 17, \dots, 100$

Sub-intervals created by the critical values of $\beta$	Order of the critical values of $C_i, i = A_1, A_2, B, D_2, D_1$
$\beta \in (0, \beta_{E_1})$	$C_B > C_{D_1} > C_{D_2} > C_{A_1} > C_{A_2}$
$\beta \in (\beta_{E_1}, \beta_{E_2})$	$C_B > C_{D_1} > C_{A_1} > C_{D_2} > C_{A_2}$
$\beta \in (\beta_{E_2}, \beta_{E_3})$	$C_B > C_{D_1} > C_{A_1} > C_{A_2} > C_{D_2}$
<b><math>\beta \in (\beta_{E_3}, \beta_{E_5})</math></b>	<b><math>C_B &gt; C_{A_1} &gt; C_{D_1} &gt; C_{A_2} &gt; C_{D_2}</math></b>
<b><math>\beta \in (\beta_{E_5}, \beta_{E_7})</math></b>	<b><math>C_{A_1} &gt; C_B &gt; C_{D_1} &gt; C_{A_2} &gt; C_{D_2}</math></b>
$\beta \in (\beta_{E_7}, \beta_N^*)$	$C_{A_1} > C_{D_1} > C_B > C_{A_2} > C_{D_2}$
$\beta > \beta_N^*$	$C_{A_1} > C_{D_1} > C_{D_2}$

The bold stands for the changes in the order of the critical values of  $\beta$  with respect to the previous tables



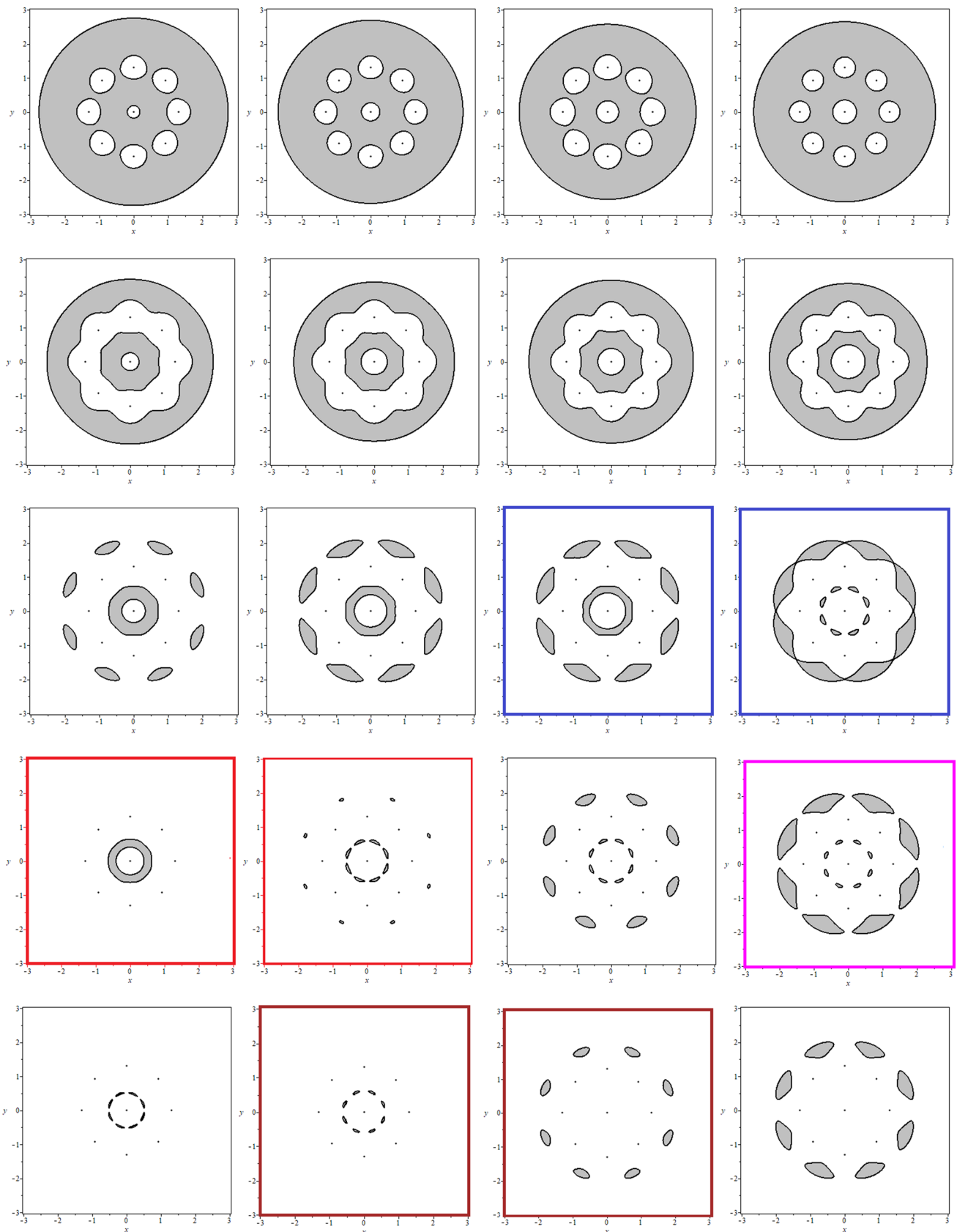


**Fig. 4** Curves of zero velocity for  $N = 8$  and  $\beta = 0.5, 0.85, 1.0, 1.4$ . From left to right and from top to bottom:  $\beta = 0.5$  and  $C = 12.0, 11.0, 10.5, 10.3, 10.194$ ;  $\beta = 0.85$  and  $C = 11.5, 10.5, 10.15, 10.015, 10.01$ ;  $\beta = 1.0$  and  $C = 11.0, 10.5, 10.0, 9.92, 9.90$ ;  $\beta = 1.4$  and  $C = 11.0, 10.0, 9.67, 9.66, 9.61$

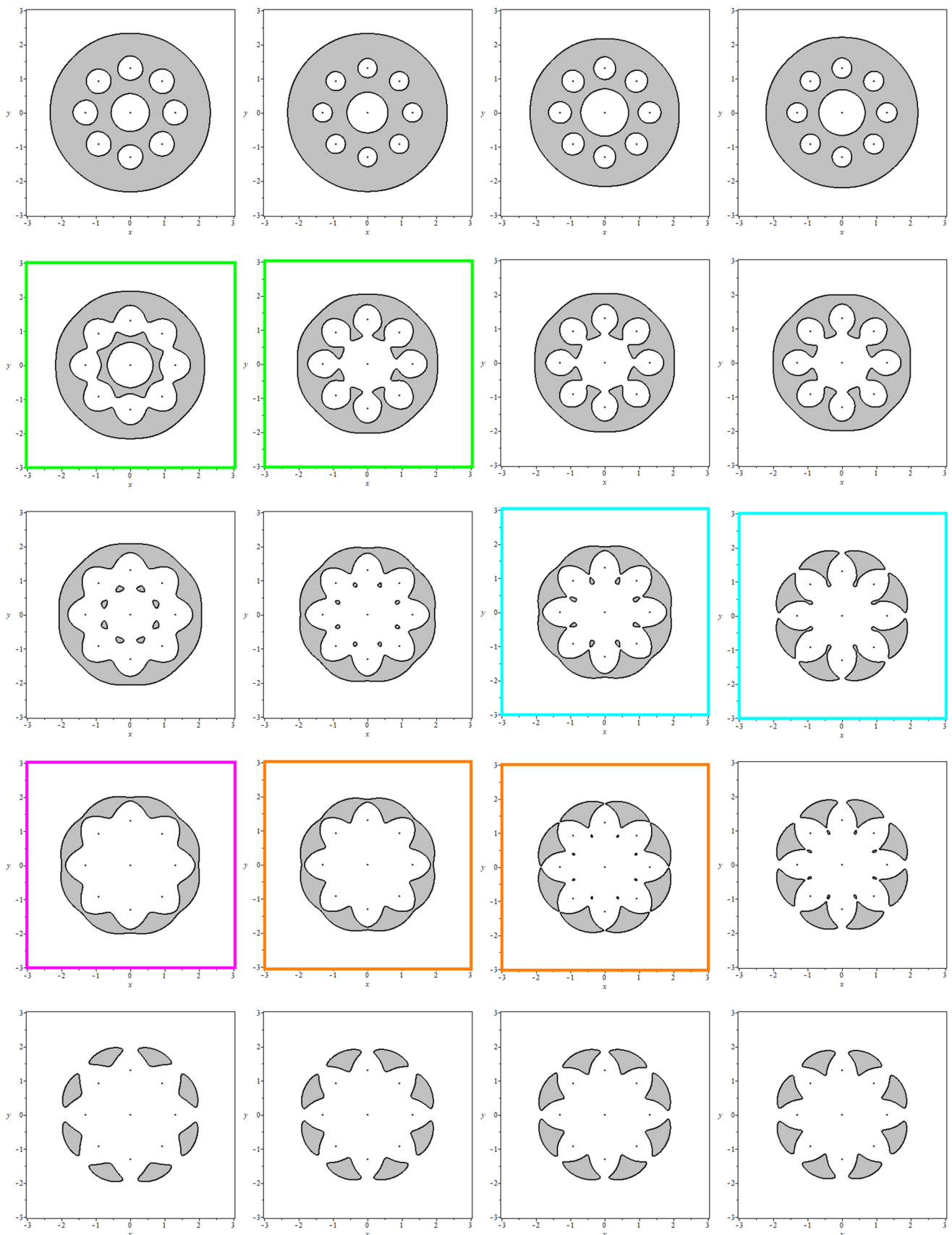


**Fig. 5** Curves of zero velocity for  $N = 8$  and  $\beta = 2.5, 4.0, 4.5, 4.9$ . From left to right and from top to bottom:  $\beta = 2.5$  and  $C = 9.5, 9.15, 9.02, 8.95, 8.9$ ;  $\beta = 4.0$  and  $C = 9.0, 8.4, 8.31, 8.29, 8.25$ ;  $\beta = 4.5$  and  $C = 8.5, 8.25, 8.13, 8.115, 8.1$ ;  $\beta = 4.9$  and  $C = 8.5, 8.1, 7.99, 7.98, 7.96$

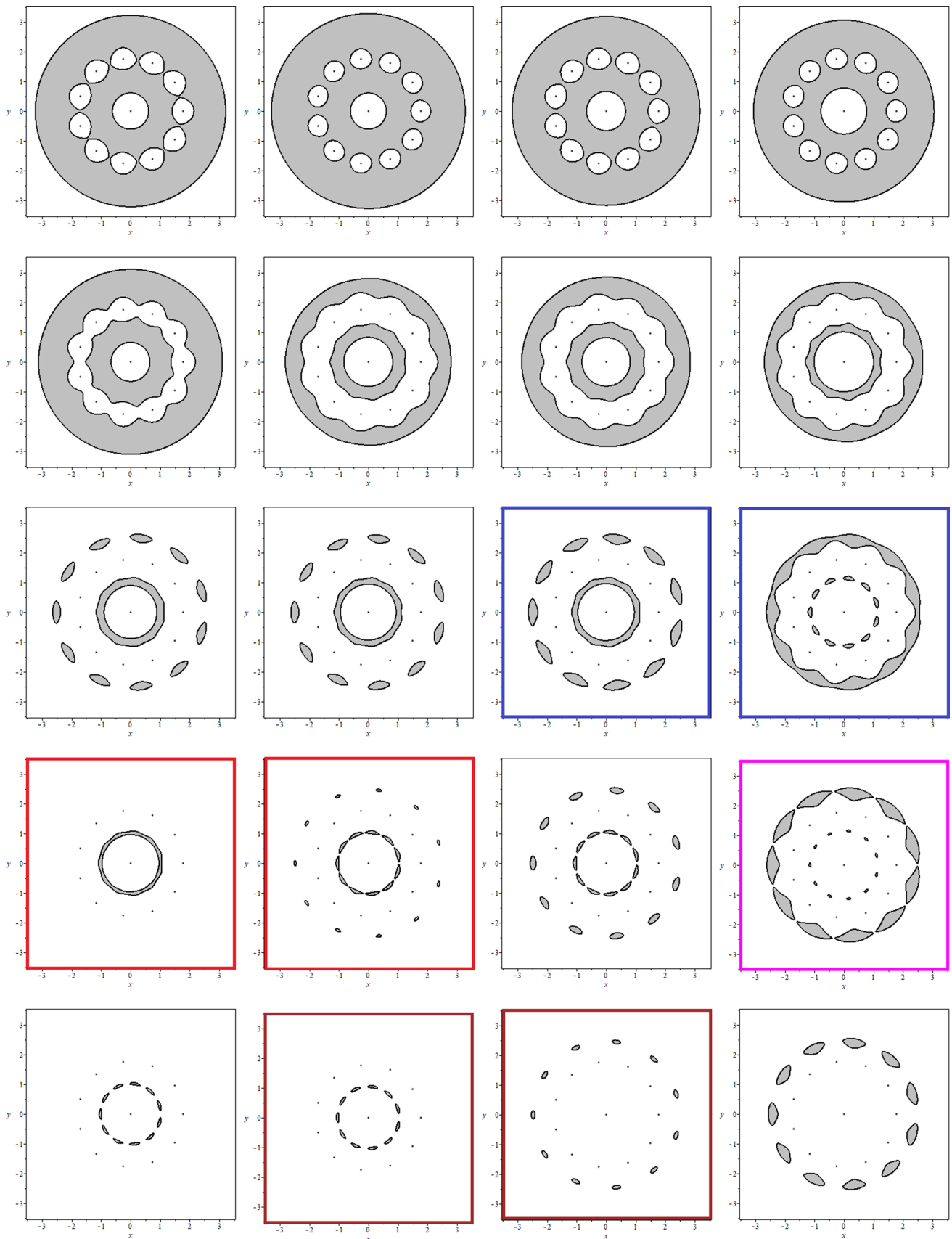


**Fig. 6** Curves of zero velocity for  $N = 11$  and  $\beta = 3.0, 3.3, 3.5, 5.0$ . From left to right and from top to bottom:  $\beta = 3.0$  and  $C = 17.4, 17.0, 15.9, 15.8, 15.78$ ;  $\beta = 3.3$  and  $C = 17.5, 16.0, 15.7, 15.637, 15.63$ ;  $\beta = 3.5$  and  $C = 17.0, 16.0, 15.6, 15.54, 15.519$ ;  $\beta = 5.0$  and  $C = 16.0, 15.0, 14.88, 14.857, 14.8$

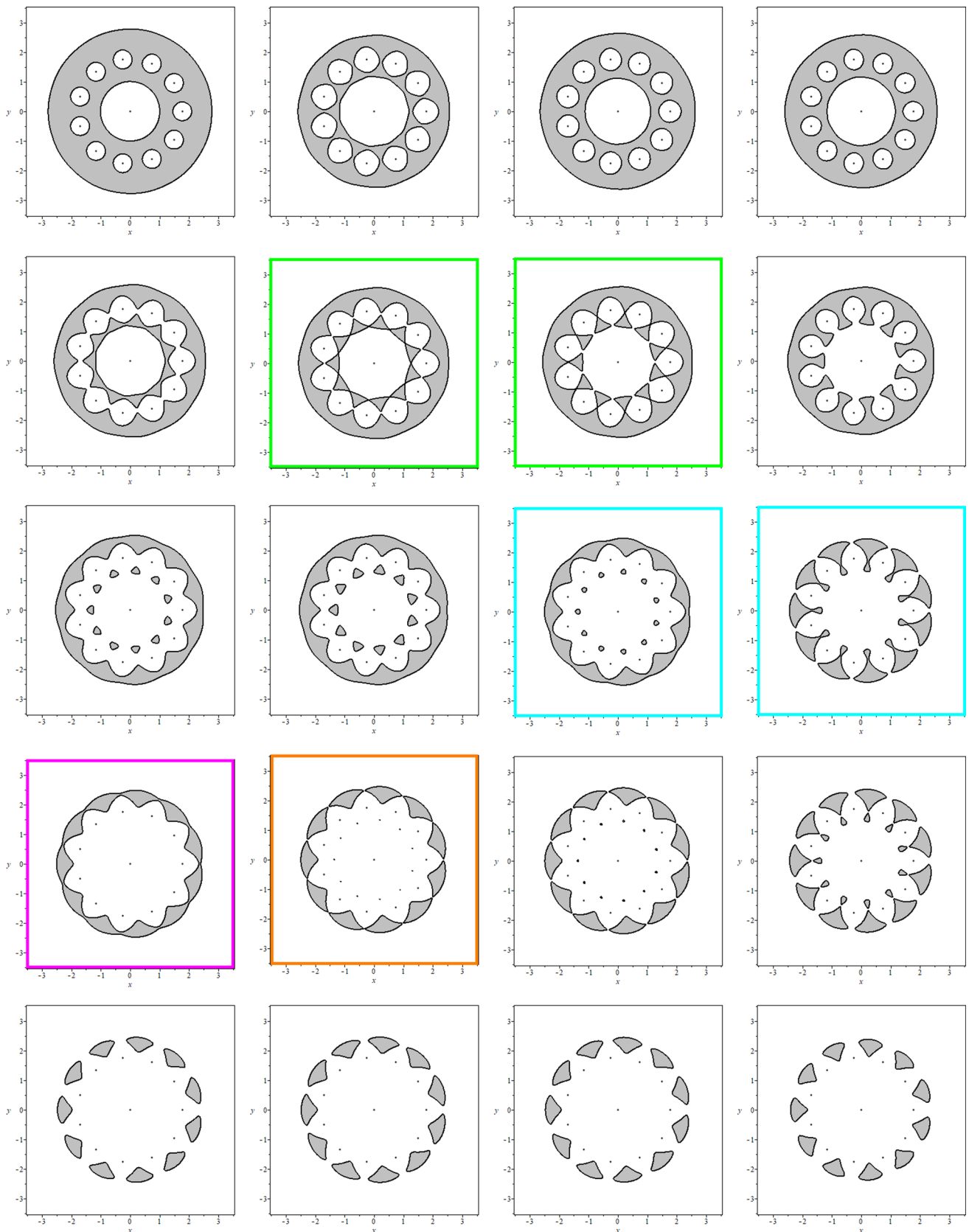


**Fig. 7** Curves of zero velocity for  $N = 11$  and  $\beta = 10.0, 10.6, 10.8, 13.47$ . From left to right and from top to bottom:  $\beta = 10.0$  and  $C = 14.0, 13.5, 13.4, 13.347, 13.3$ ;  $\beta = 10.6$  and  $C = 13.4, 13.359, 13.3, 13.219, 13.2$ ;  $\beta = 10.8$  and  $C = 13.5, 13.315, 13.2, 13.18, 13.15$ ;  $\beta = 13.8$  and  $C = 13.0, 12.8, 12.69, 12.68, 12.63$

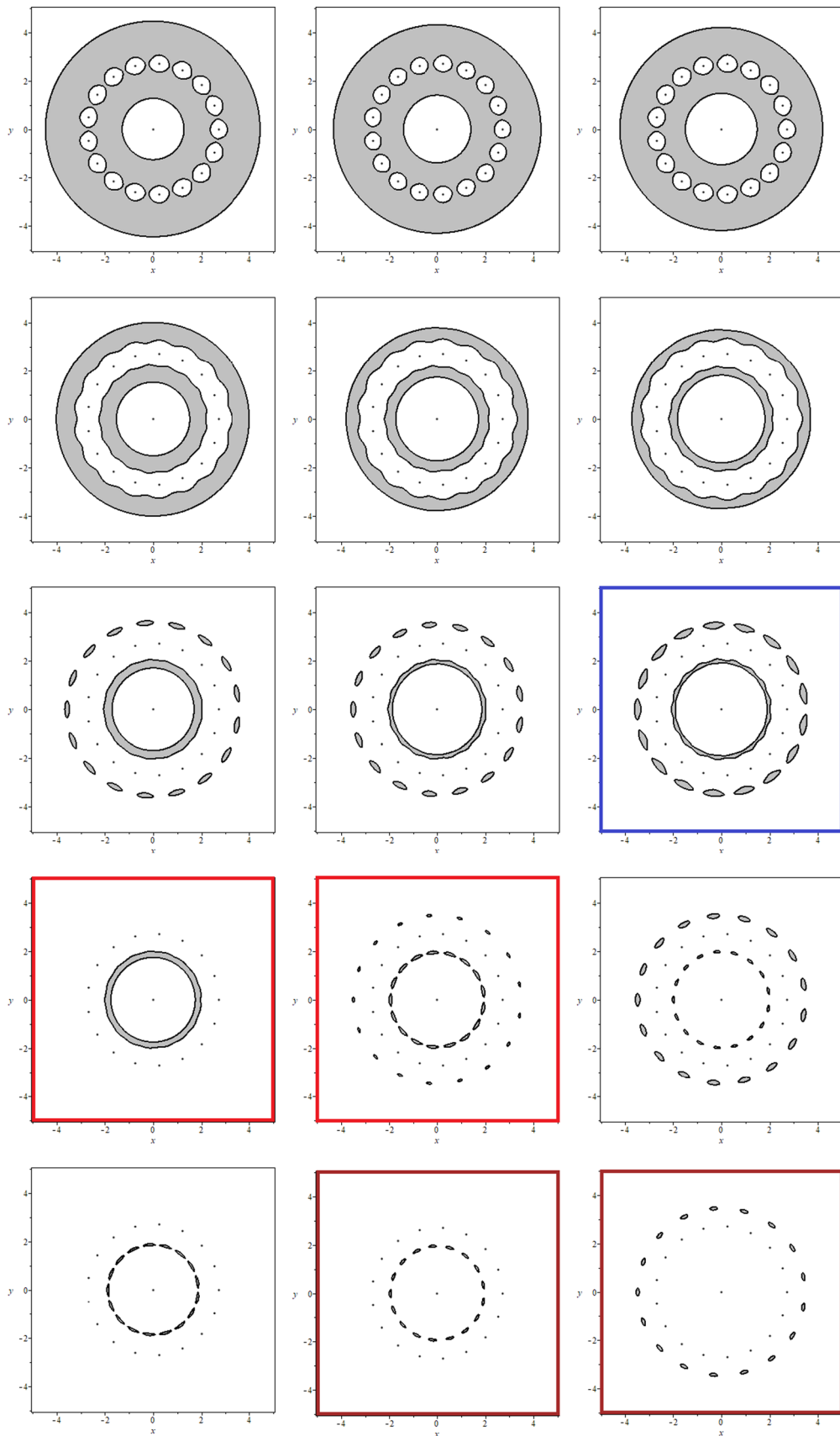


**Fig. 8** Curves of zero velocity for  $N = 17$  and  $\beta = 12.0, 15.5, 17.0$ . From left to right and from top to bottom:  $\beta = 12.0$  and  $C = 33.9, 32.0, 31.3, 31.2, 31.1$ ;  $\beta = 15.5$  and  $C = 32.4, 30.5, 30.2, 30.16, 30.15$ ;  $\beta = 17.0$  and  $C = 31.6, 30.0, 29.84, 29.8, 9.78$

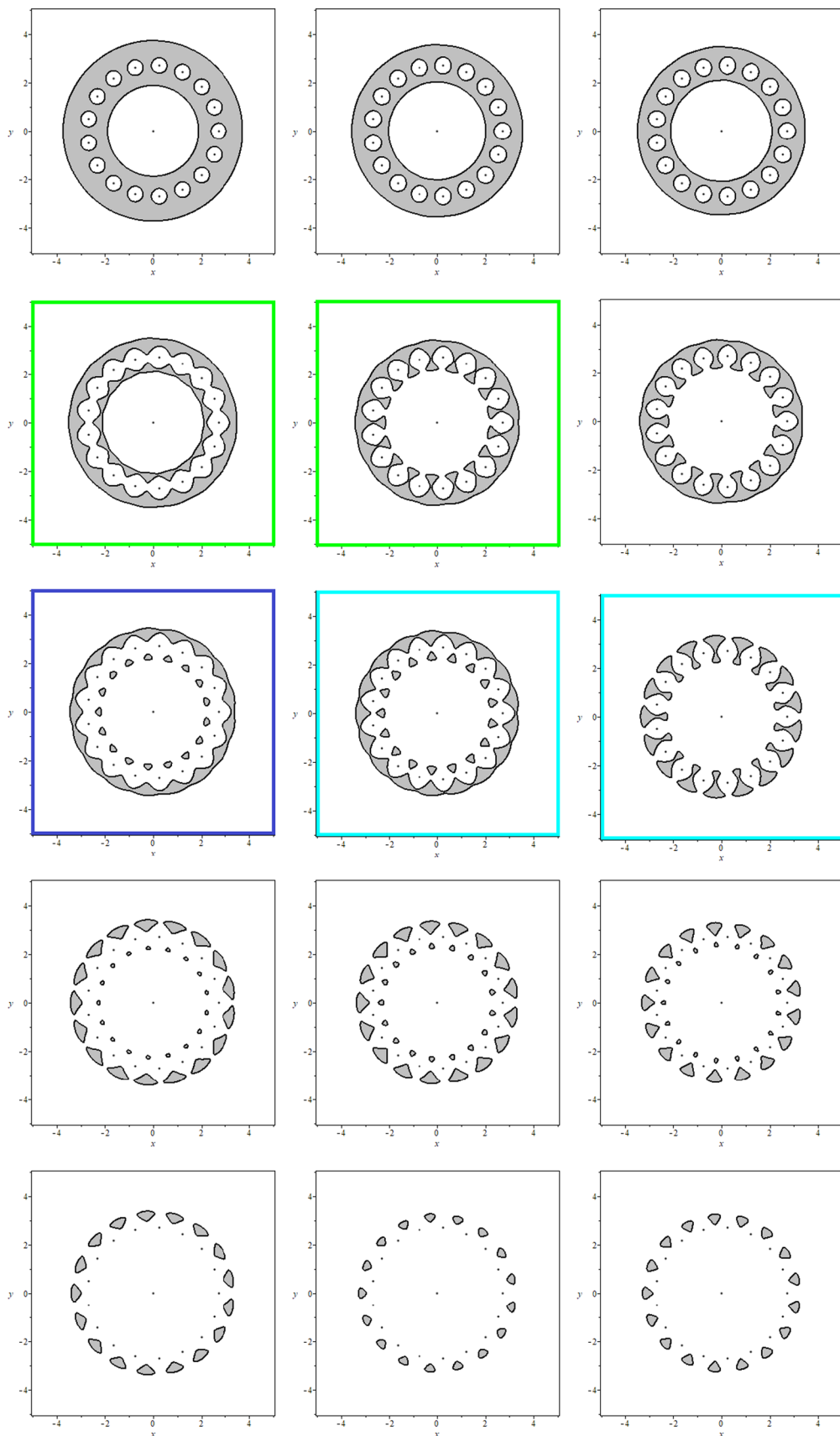


**Fig. 9** Curves of zero velocity for  $N = 17$  and  $\beta = 40, 50, 58$ . From left to right and from top to bottom:  $\beta = 40$  and  $C = 27.5, 26.9, 26.8, 26.76, 26.72$ ;  $\beta = 50$  and  $C = 26.5, 26.2, 26.15, 26.1, 26.0$ ;  $\beta = 58$  and  $C = 26.0, 25.8, 25.73, 25.67, 25.63$

- The effect of  $\beta_{E_1}$  is produced in the fourth transition, i.e., when  $C_{A_1} > C > C_{D_2}$ , highlighted in red in Fig. 4: the zero-velocity curves are totally open: the  $N$  outer islands shrink at the points of zone  $C_2$  and, at the same time, the annulus that surrounded the central body begins to decompose into small isolated islands at the locations of the stationary points that define the zone  $A_1$ . Therefore, the particle can move between the central body and the primaries and escape from the system through some of the  $N$  windows that exist.
- 3.- When  $\beta \in [\beta_{E_2}, \beta_{E_3})$ :
- The first four transitions are equivalent to the previous case.
  - The effect of  $\beta_{E_2}$  is produced in the fifth transition, i.e., when  $C_{A_2} > C > C_{D_2}$ , highlighted in brown in Fig. 4: the zero-velocity curves are also open but there is a shift in their shape with respect to the preceding case: the small inner isolated islands disappear whereas the  $N$  outer larger islands remain.
- 4.- When  $\beta \in [\beta_{E_3}, \beta_{E_4})$ :
- The first two transitions are equivalent to the previous cases.
  - The effect of  $\beta_{E_3}$  is produced in the third transition, i.e., when  $C_{A_1} > C > C_{D_1}$ , highlighted in blue in Fig. 4: the annulus that surrounded the central body is decomposed into  $N$  small isolated islands, at the locations of the points of the zone  $A_1$ , but the zero-velocity curves are still closed, then, the particle may move between the central body and the primaries, but it cannot escape from the system.
  - The zero-velocity curves open in the fourth transition and their evolution to the fifth transition is similar to case number 3.
- 5.- When  $\beta \in [\beta_{E_4}, \beta_{E_5})$ :
- The first two transitions are similar to all the previous cases.
  - The third and fifth transitions follow the same pattern as the case described in item number 4.
  - The effect of  $\beta_{E_4}$  is produced in the fourth transition, i.e., when  $C_{A_2} > C > C_{D_1}$ , highlighted in violet pink in Figs. 4 and 5: the  $N$  inner small isolated islands disappear, but the zero-velocity curves remain closed so that the particle is trapped, and it can move only between the primaries and the central body.
- 6.- When  $\beta \in [\beta_{E_5}, \beta_{E_6})$ :
- The behavior of the zero-velocity curves is similar in transitions one and three to five.
  - The effect of  $\beta_{E_5}$  is produced in the second transition, i.e., when  $C_{A_1} > C > C_B$ , highlighted in green in Fig. 5: the zero-velocity curves are still closed, but the central annulus disappears, and the inner curves of the zero-velocity curves merge at the location of the points of zone  $B$ , creating  $N$  small openings that allow the particle to move between the central body and the primaries.
- 7.- When  $\beta \in [\beta_{E_6}, \beta_{E_7})$ :
- Transitions one to three and five are similar to the preceding case.
  - The effect of  $\beta_{E_6}$  is produced in the fourth transition, i.e., when  $C_{D_1} > C > C_{A_2}$ , highlighted in orange in Fig. 5: the external forbidden area shrinks and splits up into  $N$  windows, at the location of the points of zone  $C_1$ , through which the particle may escape, but there are still  $N$  small islands between the primaries at the location of the points of zone  $A_2$ .
- 8.- When  $\beta \in [\beta_{E_7}, \beta_N^*)$ :
- In this last case there is a change in the evolution of the zero-velocity curves in the third transition with respect to the previous case, that is, when  $C_{D_1} > C > C_B$ , highlighted in cyan in Fig. 5: they open at this stage, as the external forbidden area shrinks and forms  $N$  islands, creating  $N$  windows at the location of the points of zone  $D_1$ . Then, the particle may escape through them.

An example of this behavior is illustrated in Figs. 4 and 5, for  $N = 8$  and several values of  $\beta$ .

#### 4.2.2 Scenario with $11 \leq N \leq 16$

There is only a change in the order of appearance of the intersections that define  $\beta_{E_5}$  and  $\beta_{E_6}$ ; hence, the effects described in the zero-velocity curves defined in items 6 and 7 when  $N < 11$  are shifted (see Tables 3, 4, and 5 and Figs. 6 and 7).

#### 4.2.3 Scenario with $17 \leq N \leq 100$

Due to the fact that  $\beta_{E_4}$  and  $\beta_{E_6}$  do not exist in this case (then, zones  $D_1$  and  $A_2$  do not intersect) there are  $N$  small isolated islands present simultaneously with the opening of the  $N$  windows during the fourth transition (see Figs. 8 and 9).

## 5 Conclusions

In this research, we have carried out a qualitative analysis of the shape of the zero-velocity curves (which bound the regions of possible motion of the test particle) in the planar  $N$ -body ring problem for  $N = 3, 4, \dots, 100$  peripheral bodies with the presence of a central body ( $\beta > 0$ ). For this purpose, we have accomplished a very accurate analysis of the different intersections of the so-called critical values of the Jacobi constant, which characterize the sets of stationary points of the system, when  $\beta$  is lower than the bifurcation value of the system,  $\beta_N^*$ . As a result, we have found that there can be up to a maximum of seven intersections between these critical values, which are directly related to a particular value of  $\beta$ , here denoted as  $\beta_{E_i}$ ,  $i = 1, 2, \dots, 7$ . We have shown that each of these  $\beta_{E_i}$  produces a specific change in the arrangement of the critical values of the Jacobi constant, which then involve a different evolution of the shape of the zero-velocity curves for decreasing values of the constant of Jacobi. The number of these critical values of  $\beta$  is not constant with  $N$ , that is, there is a relation between the number of peripheral bodies and the behavior of the intersections of the different zones of stationary solutions. It has also been shown that there is not intersection between the zones  $A_2$  and  $D_1$  when  $N > 16$ , which causes that the small isolated islands around the central mass have not still disappeared when the zero-velocity curves open. Finally, due to the fact that the set  $\{z = 0, \dot{z} = 0\}$  is invariant in this system, the results of this research can be applied to explain the motion of an infinitesimal particle that lies on the  $XY$  plane in the  $3D$   $N$ -body ring problem, which we can then conclude that will be subject to the same structure of the zero-velocity curves in the plane.

**Funding** Open Access funding provided thanks to the CRUE-CSIC agreement with Springer Nature. This work has been partially funded by the Algerian Ministry of Higher Education and Scientific Research, who awarded a grant for PhD training abroad in 2020 to the first author, Zahra Boureghda, at the University of Alicante.

**Data Availability** There is no data associated in the manuscript.

## Declarations

**Conflict of interest** The authors declare no potential conflict of interests.

**Open Access** This article is licensed under a Creative Commons Attribution 4.0 International License, which permits use, sharing, adaptation, distribution and reproduction in any medium or format, as long as you give appropriate credit to the original author(s) and the source, provide a link to the Creative Commons licence, and indicate if changes were made. The images or other third party material in this article are included in the article's Creative Commons licence, unless indicated otherwise in a credit line to the material. If material is not included in the article's Creative Commons licence and your intended use is not permitted by statutory regulation or exceeds the permitted use, you will need to obtain permission directly from the copyright holder. To view a copy of this licence, visit <http://creativecommons.org/licenses/by/4.0/>.

## References

1. M. Woodard, D. Folta, D. Woodfork, Artemis: the first mission to the lunar libration orbits. In: Proc. of the 21st International Symposium on Space Flight Dynamics, Toulouse, France (2009)
2. A. Knutson, K. Howell, Coupled orbit and attitude dynamics for spacecraft composed of multiple bodies in earth-moon halo orbits. Proc. of the International Astronautical Congress, IAC. **8**, 5951–5965 (2012)
3. E. Canalias, J.J. Masdemont, Homoclinic and heteroclinic transfer trajectories between planar Lyapunov orbits in the sun-earth and earth-moon systems. Discrete Contin. Dyn. Syst. **14**(2), 261–279 (2006)
4. W.S. Koon, M.W. Lo, J.E. Marsden, S.D. Ross, Dynamical Systems, the Three-Body problem and Space Mission Design. Equadiff **99**, 1167–1181 (2000)
5. J.C. Maxwell, *On the stability of motions of Saturn's rings* (Macmillan and Company, Cambridge, 1859)
6. H. Salo, C.F. Yoder, The dynamics of coorbital satellite systems. Astron. Astrophys. **205**, 309–327 (1988)
7. F. Tisserand, *Traité de Mécanique Céleste* (Tome II. Gauthier-Villars, Paris, 1889)
8. T.J. Kalvouridis, A planar case of the  $n + 1$  body problem: the 'ring' problem. Astrophys. Space Sci. **260**, 309–325 (1999)
9. T.J. Kalvouridis, A planar case of the  $n + 1$  body problem: the 'ring' problem. Periodic Solut. Ring Problem **266**, 467–494 (1999)
10. M. Arribas, A. Elipe, Bifurcations and equilibria in the extended  $n$ -body ring problem. Mech. Res. Commun. **31**(1), 1–8 (2004)
11. T.J. Kalvouridis, On a property of zero-velocity curves in  $n$ -body ring-type systems. Planet. Space Sci. **52**, 909–914 (2004)
12. M.N. Croustalloudi, T.J. Kalvouridis, Regions of a satellite's motion in a Maxwell's ring system of  $n$  bodies. Astrophys. Space Sci. **331**, 497–510 (2011)
13. R. Barrio, F. Blesa, S. Serrano, Qualitative analysis of the  $(n + 1)$ -body ring problem. Chaos Solit. Fractals **36**(4), 1067–1088 (2008)
14. E. Barrabés, J.M. Cors, G.R. Hall, Numerical exploration of the limit ring problem. Qual. Theory Dyn. Syst. **12**, 25–52 (2013)
15. J.F. Navarro, M.C. Martínez-Belda, Escaping orbits in the  $n$ -body ring problem. Comput. Math. Methods **2**(1), 1067 (2020)
16. J.F. Navarro, M.C. Martínez-Belda, On the use of surfaces of section in the  $n$ -body ring problem. Math. Methods Appl. Sci. **43**(5), 2289–2300 (2020)
17. J.F. Navarro, M.C. Martínez-Belda, On the analysis of the fractal basins of escape in the  $n$ -body ring problem. Comput. Math. Methods **3**(6), 1131 (2021)
18. J.F. Navarro, M.C. Martínez-Belda, Analysis of the distribution of times of escape in the  $n$ -body ring problem. J. Comput. Appl. Math. **404**, 113396 (2022)
19. M.S. Suraj, R. Aggarwal, A. Mittal, O.P. Meena, M.C. Asique, The study of the fractal basins of convergence linked with equilibrium points in the perturbed  $(n + 1)$ -body ring problem. Astron. Nachr. **341**(8), 741–761 (2020)



20. T.J. Kalvouridis, K.G. Hadjifotinou, Particle dynamics in a Maxwell's ring-type configuration with a radiating central primary. *Earth Moon Planet.* **108**, 51–67 (2011)
21. T.J. Kalvouridis, J. Telemachus, The effect of radiation pressure on the particle dynamics in ring-type N-body configurations. *Earth Moon Planet.* **87**, 87–102 (1999)
22. V. Szebehely, *Theory of orbits: The Restricted Problem of Three Bodies* (Academic Press Inc., New York, 1967)
23. D.J. Scheeres, On symmetric central configurations with application to satellite motion about rings. Ph.D. thesis, University of Michigan (1992)
24. D.J. Scheeres, N.X. Vinh, The restricted  $p + 2$  body problem. *Acta Astron.* **29**(4), 237–248 (1993)
25. K.E. Papadakis, Asymptotic orbits in the  $(n + 1)$ -body ring problem. *Astrophys. Space Sci.* **323**, 261–272 (2009)